Manuscript Type: **Research Article**
Submitted to: **New Journal of Chemistry**
Article number: **NJ-ART-01-2026-000257**

Supplementary Information

Nickel(II)-Flavonolate Complexes of Tetradentate 4N Donor Ligands as Enzyme-Substrate Models of Quercetin-2,4-Dioxygenase: Role of Ligand Steric and Electronic Properties on Dioxygenolysis

*Devaraj Karthickram[a], Nattamai Bhuvanesh[b] and Karuppasamy Sundaravel[a]**

[a]Bioinorganic Research Laboratory, Department of Chemistry, Bharathiar University, Coimbatore - 641046, Tamil Nadu, India.

[b]X-ray Diffraction Laboratory, Texas A&M University, College Station, TX 77842, United States of America.

* To whom correspondence should be addressed E-mail: sundaravel.k@gmail.com, sundaravel.k@buc.edu.in
Tel: +91-82207 17342

Table of Contents

Figure S1

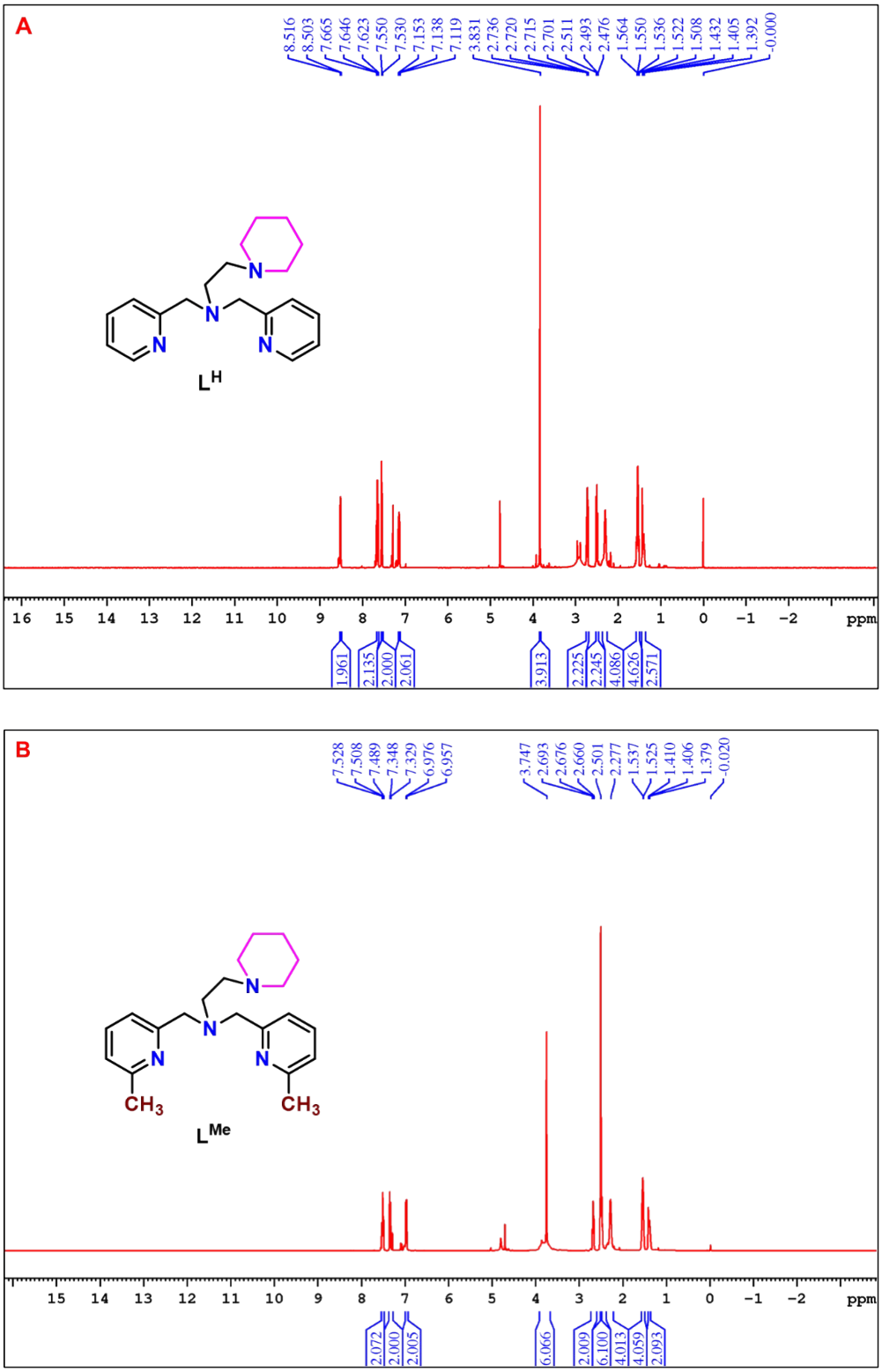

Fig. S1 ^{1}H NMR spectra of ligands (A) L^{H} and (B) L^{Me} in $CDCl_3$ at 298 K.

Figure S2

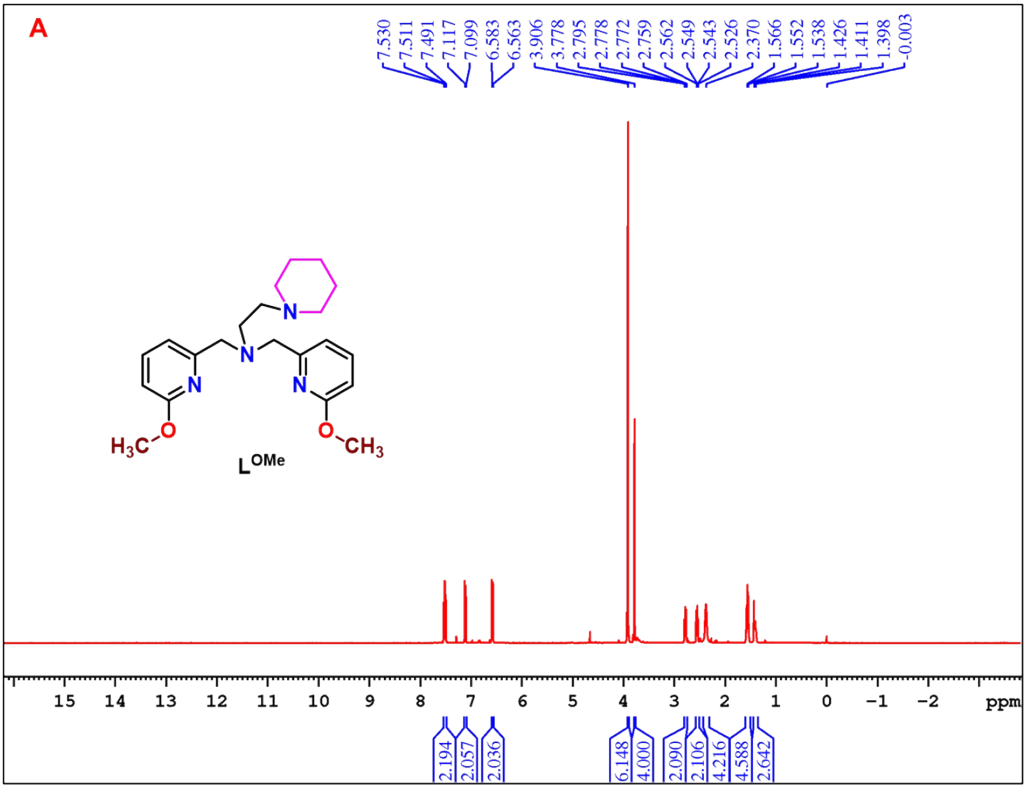
A
7.530
7.511
7.491
7.117
7.099
6.583
6.563
3.906
3.778
2.795
2.778
2.772
2.759
2.562
2.549
2.543
2.526
2.370
1.566
1.552
1.538
1.426
1.411
1.398
-0.003
N
N
N
N
H3C
O
O
CH3
LOMe
15 14 13 12 11 10 9 8 7 6 5 4 3 2 1 0 −1 −2 ppm
2.194
2.057
2.036
6.148
4.000
2.090
2.106
4.216
4.588
2.642

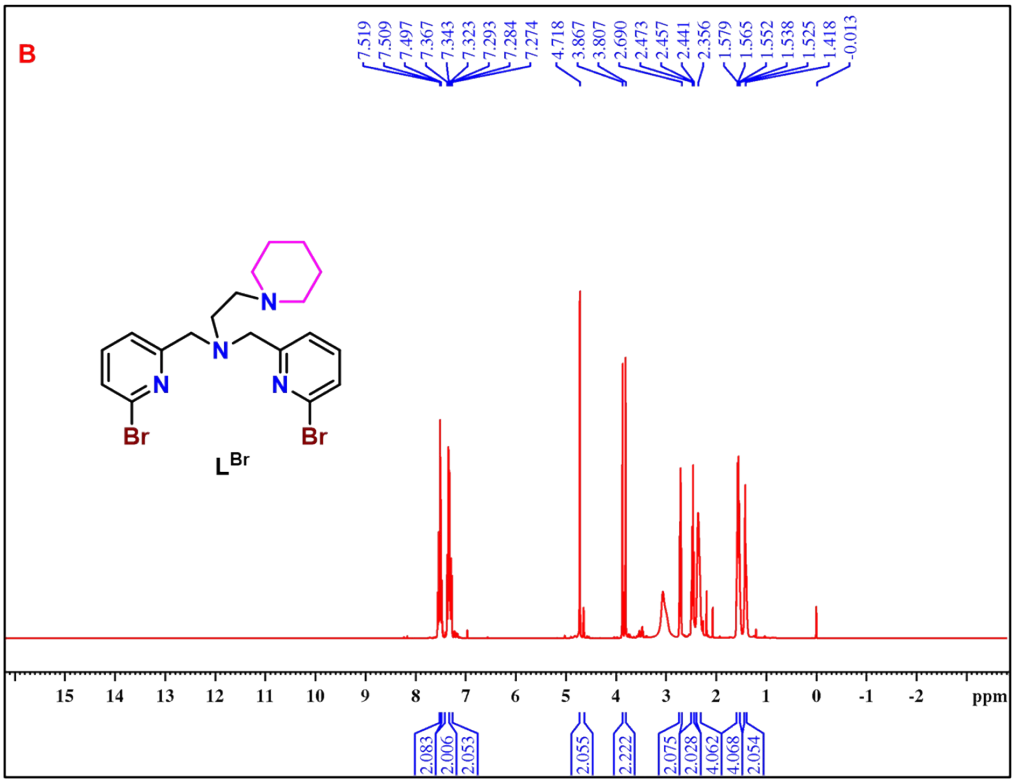
B
7.519
7.509
7.497
7.367
7.343
7.323
7.293
7.284
7.274
4.718
3.867
3.807
2.690
2.473
2.457
2.441
2.356
1.579
1.565
1.552
1.538
1.525
1.418
-0.013
N
N
N
N
Br
Br
LBr
15 14 13 12 11 10 9 8 7 6 5 4 3 2 1 0 -1 -2 ppm
2.083
2.006
2.053
2.055
2.222
2.075
2.028
4.062
4.068
2.054

Fig. S2 ^{1}H NMR spectra of ligands (A) $\mathbf{L^{OMe}}$ and (B) $\mathbf{L^{Br}}$ in $CDCl_3$ at 298 K.

Figure S3

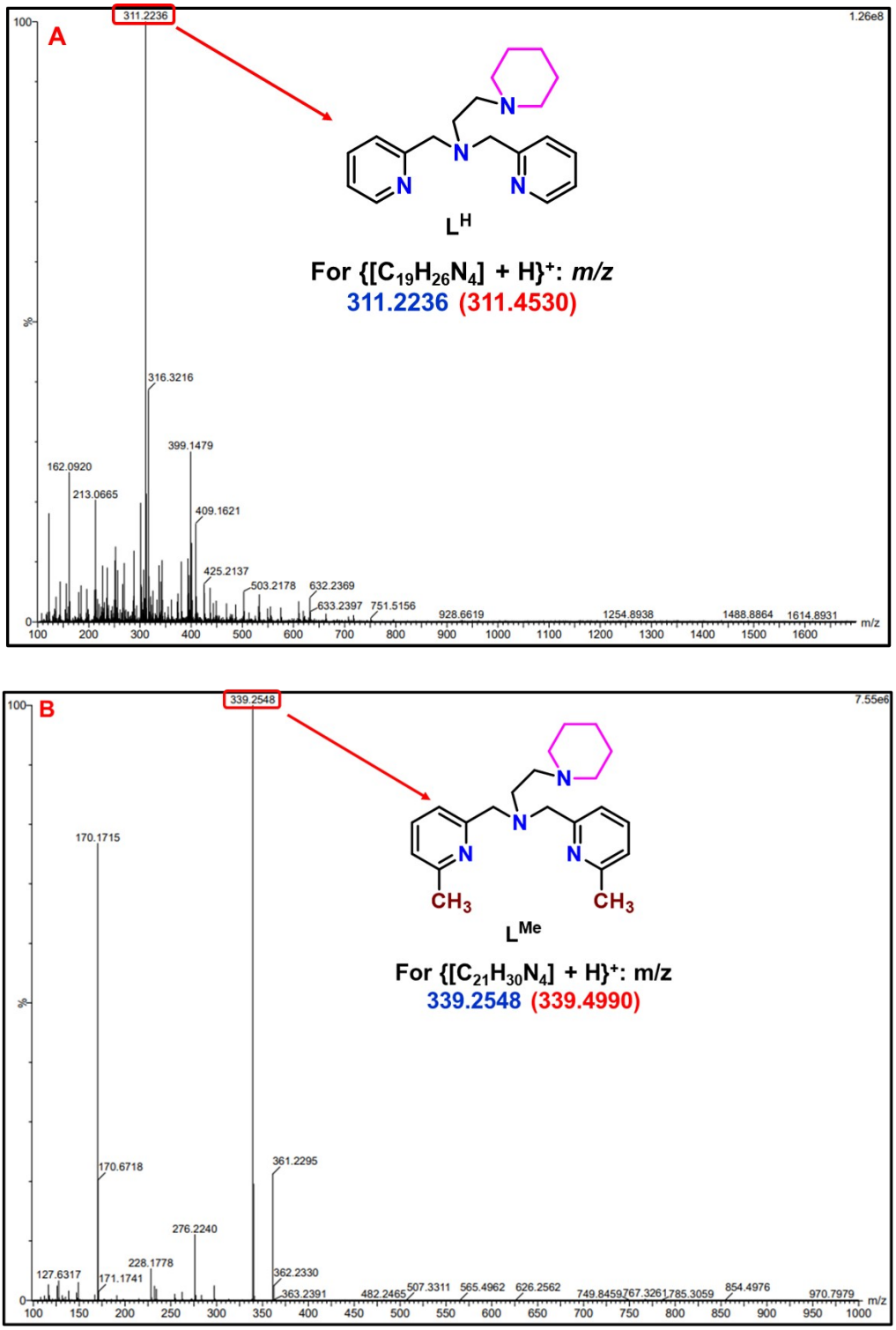

Fig. S3 ESI-MS spectral profiles of complexes (A) $\mathbf{L^{H}}$ and (B) $\mathbf{L^{Me}}$ recorded in CH_3OH.

Figure S4

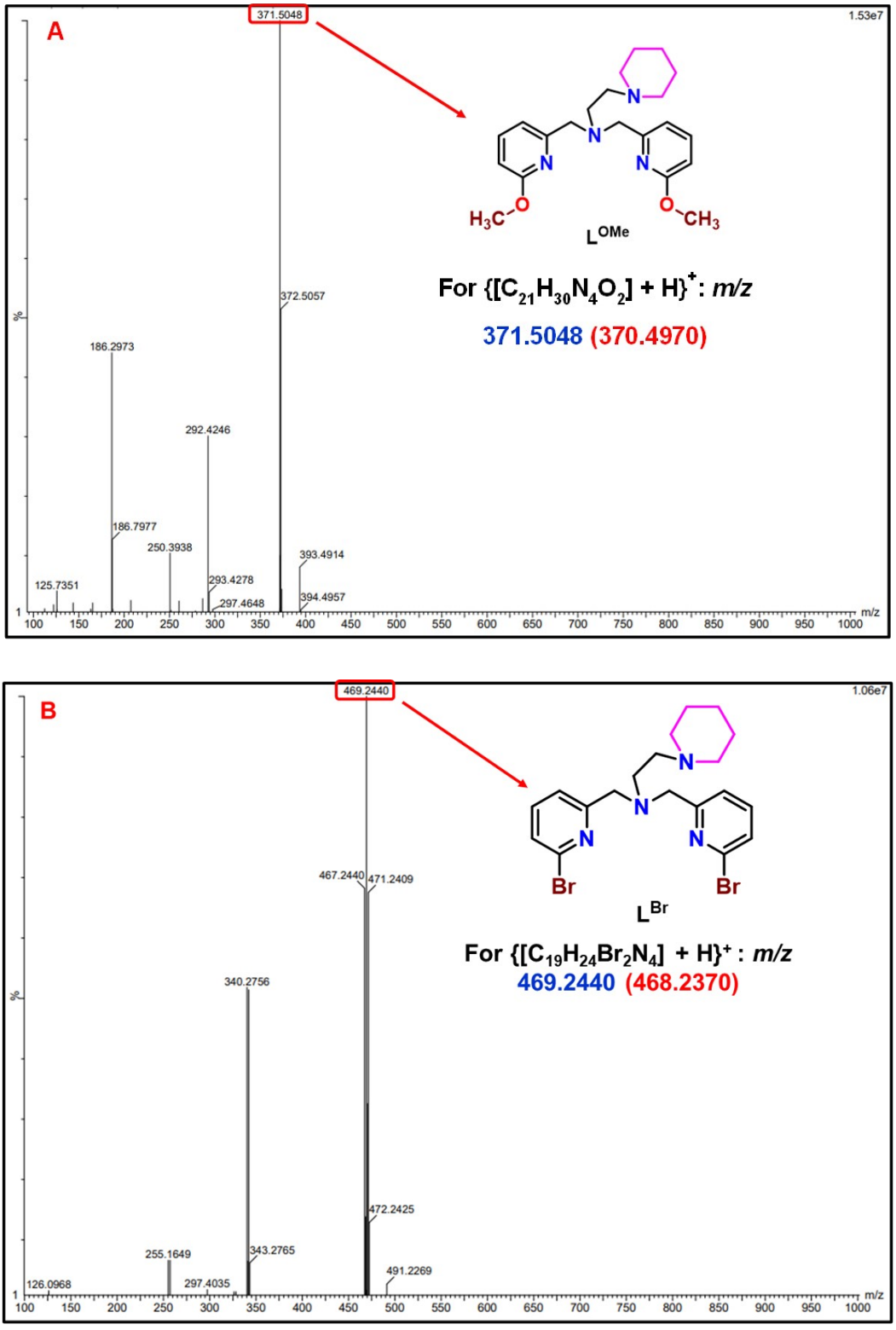

Fig. S4 ESI-MS spectral profiles of complexes (A) $\mathbf{L^{OMe}}$ and (B) $\mathbf{L^{Br}}$ recorded in CH_3OH.

Figure S5

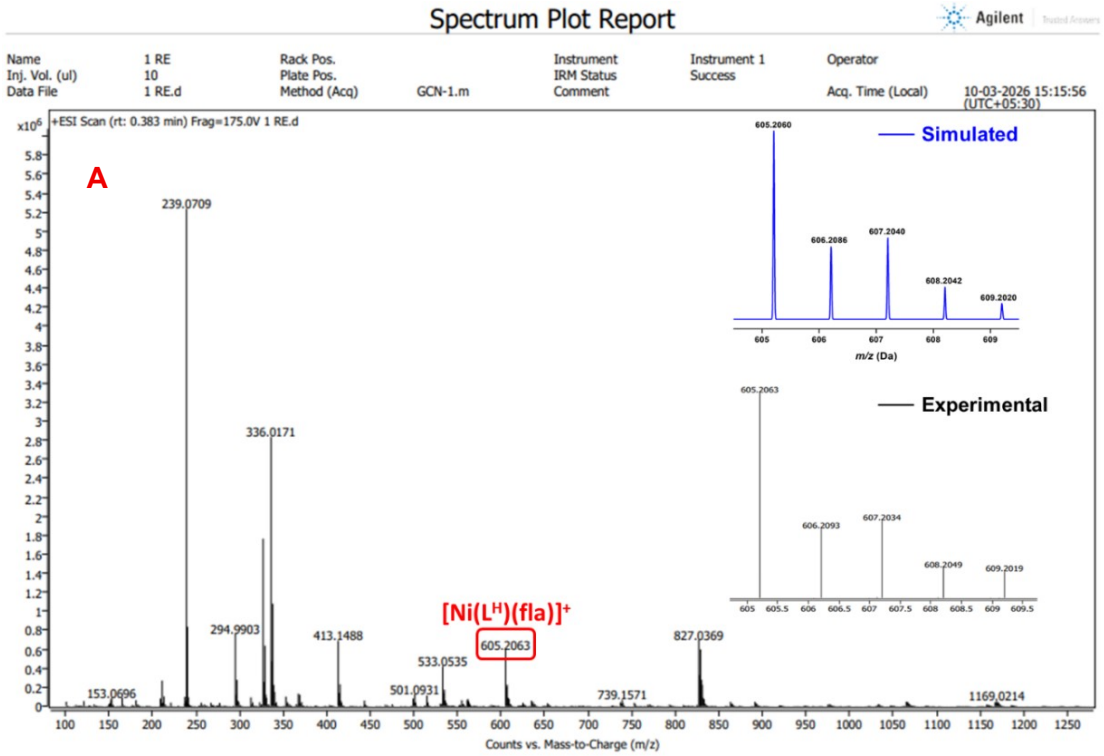
Spectrum Plot Report
Agilent
Name 1 RE
Inj. Vol. (ul) 10
Data File 1 RE.d
Rack Pos.
Plate Pos.
Method (Acq) GCN-1.m
Instrument
IRM Status
Comment
Instrument 1
Success
Operator
Acq. Time (Local) 10-03-2026 15:15:56 (UTC+05:30)
+ESI Scan (rt: 0.383 min) Frag=175.0V 1 RE.d
A
239.0709
336.0171
294.9903
413.1488
533.0535
605.2063
501.0931
739.1571
827.0369
153.0696
1169.0214
[Ni(L^H)(fla)]+
Simulated
Experimental
m/z (Da)
Counts vs. Mass-to-Charge (m/z)

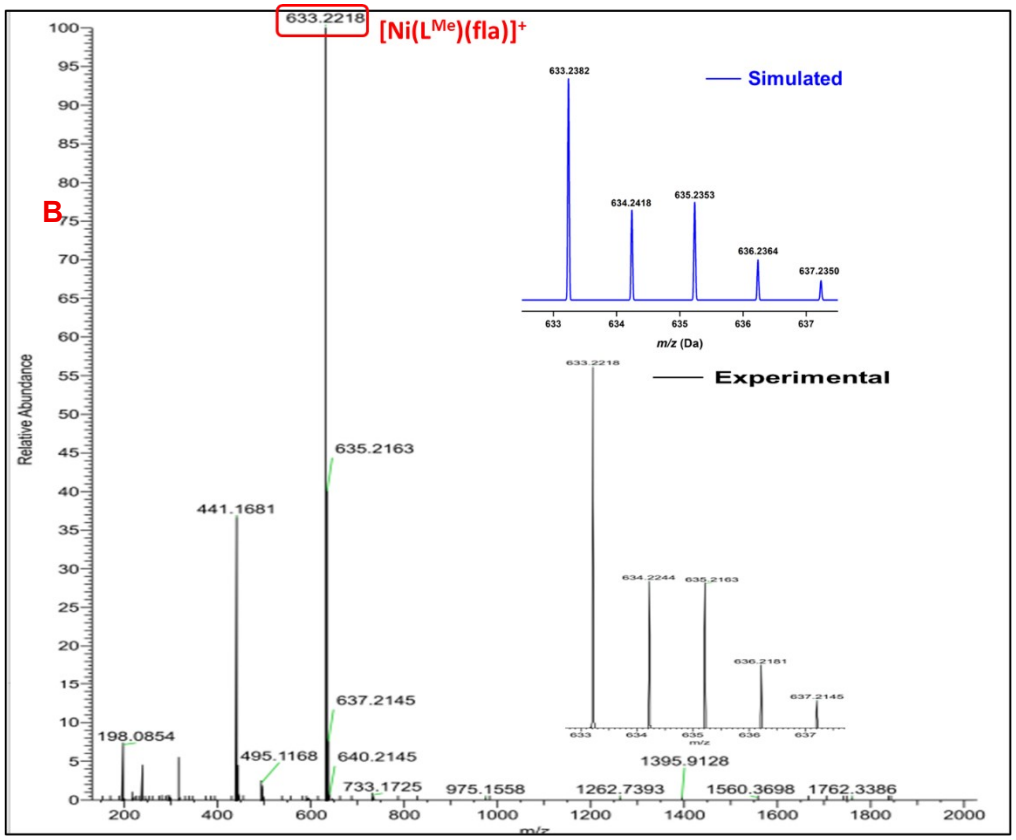
633.2218
[Ni(L^Me)(fla)]+
B
Simulated
Experimental
m/z (Da)
Relative Abundance
635.2163
441.1681
637.2145
198.0854
495.1168
640.2145
733.1725
975.1558
1262.7393
1395.9128
1560.3698
1762.3386
m/z

Fig. S5 ESI-MS profiles of E-S model adducts (A) [Ni($\mathbf{L^H}$)(fla)]ClO_4 **1** and (B) [Ni($\mathbf{L^{Me}}$)(fla)]ClO_4 **2** recorded in CH_3OH. Inset shows the simulated and experimental isotopic distribution pattern of complexes.

Figure S6

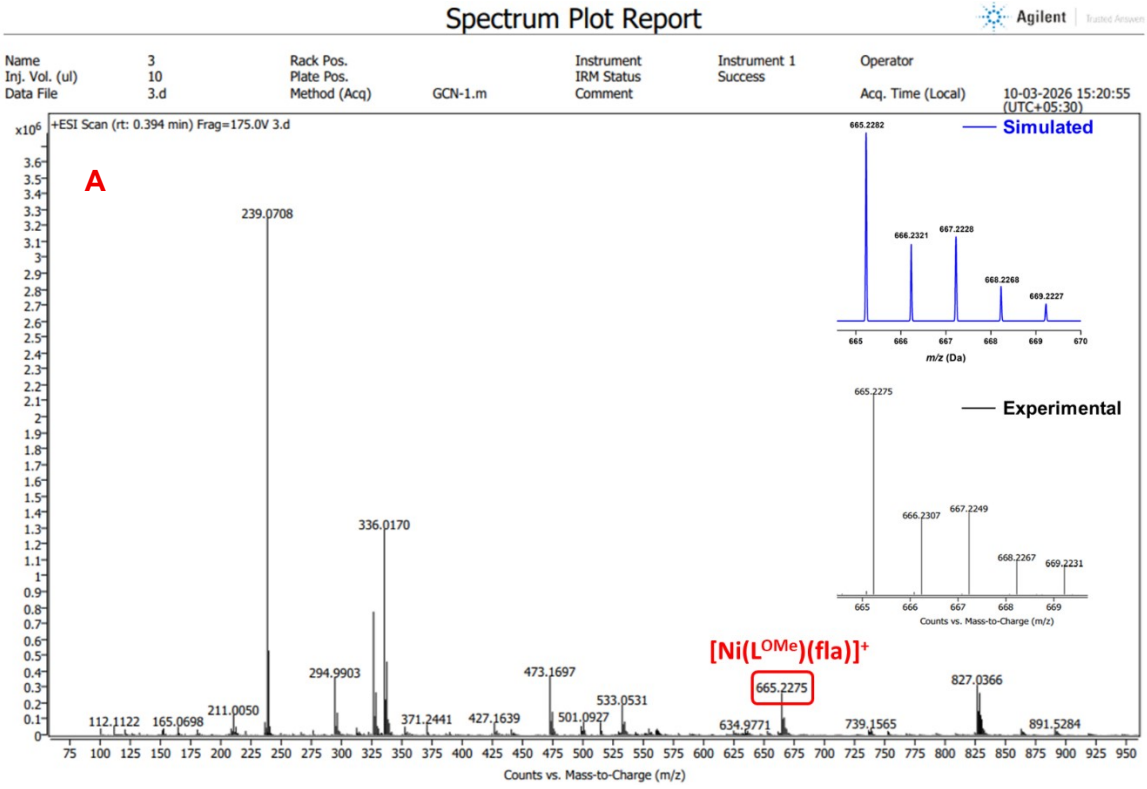

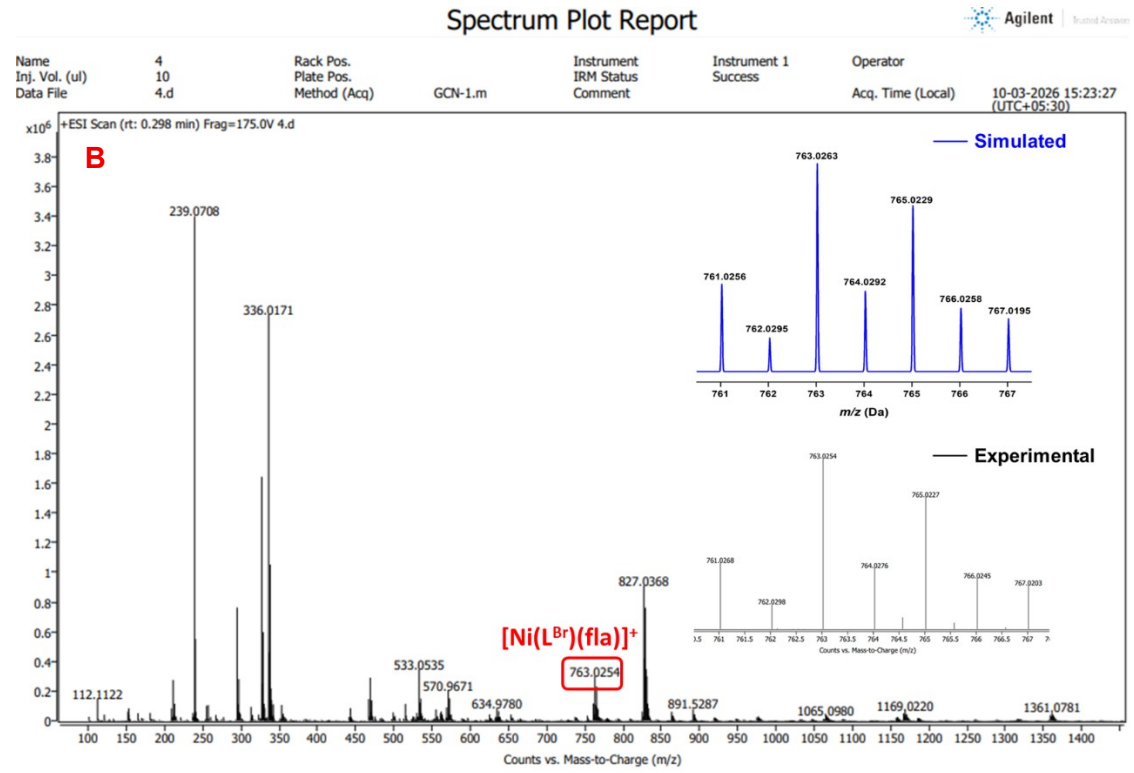

Fig. S6 ESI-MS profile of E-S model adducts (A) [Ni($\mathbf{L^{OMe}}$)(fla)]ClO_4 **3** and (B) [Ni($\mathbf{L^{Br}}$)(fla)]ClO_4 **4** recorded in CH_3OH. Inset shows the simulated and experimental isotopic distribution pattern of complexes.

Figure S7

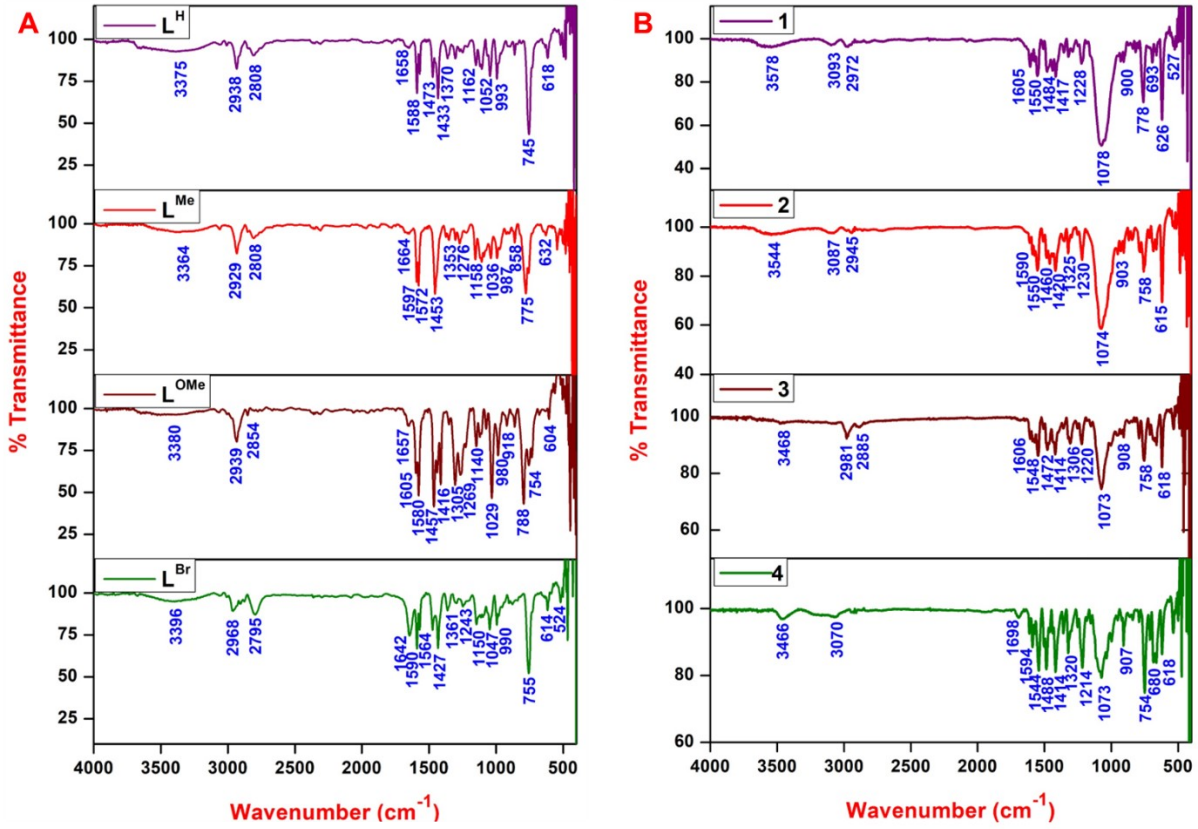

Fig. S7 ATR-FTIR spectra of ligands $\mathbf{L^H}$–$\mathbf{L^{Br}}$ (A) and nickel(II)-flavonolate adducts **1**–**4** (B).

Figure S8

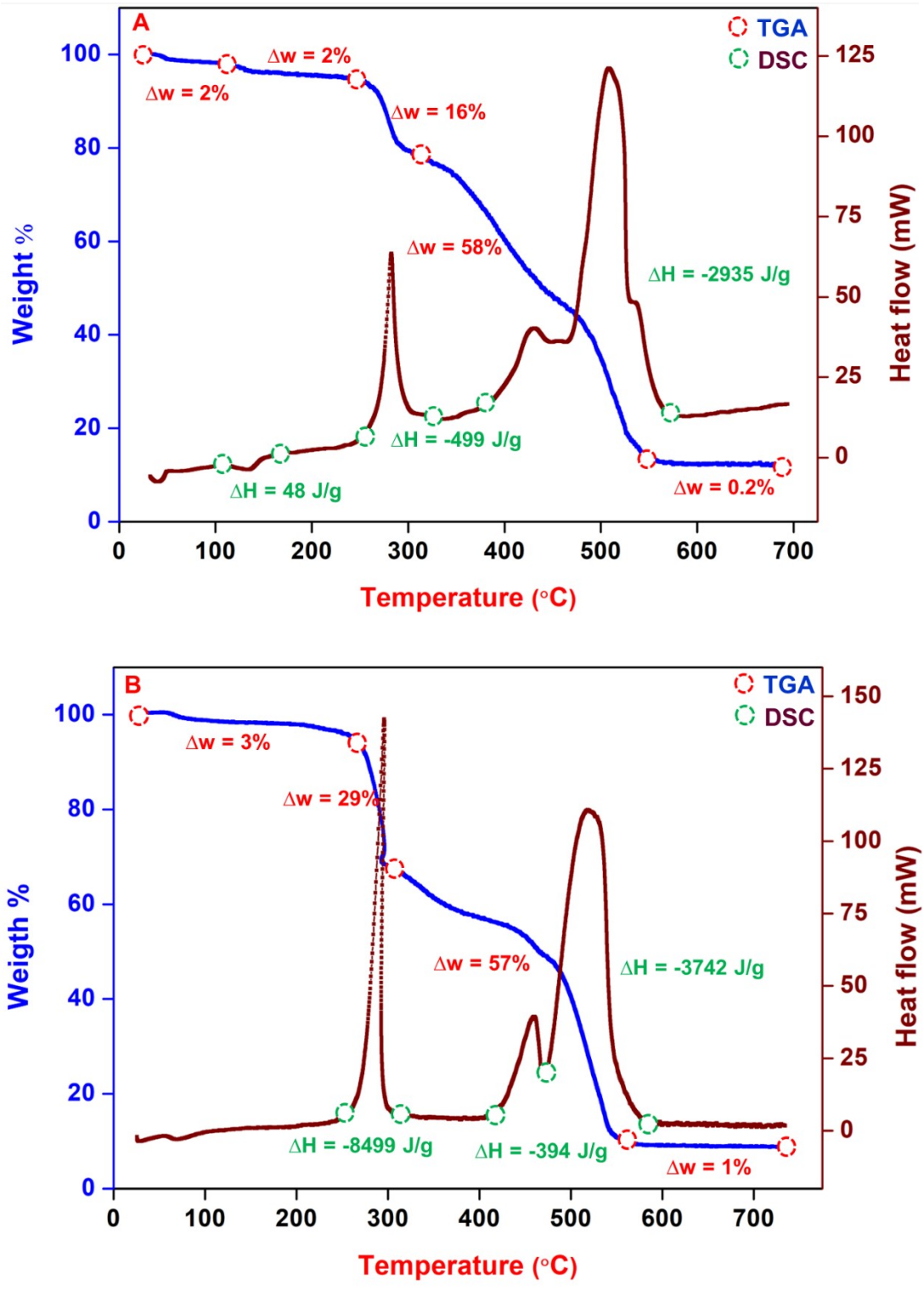

Fig. S8 TG-DSC profiles of (A) **1** and (B) **2**.

Figure S9

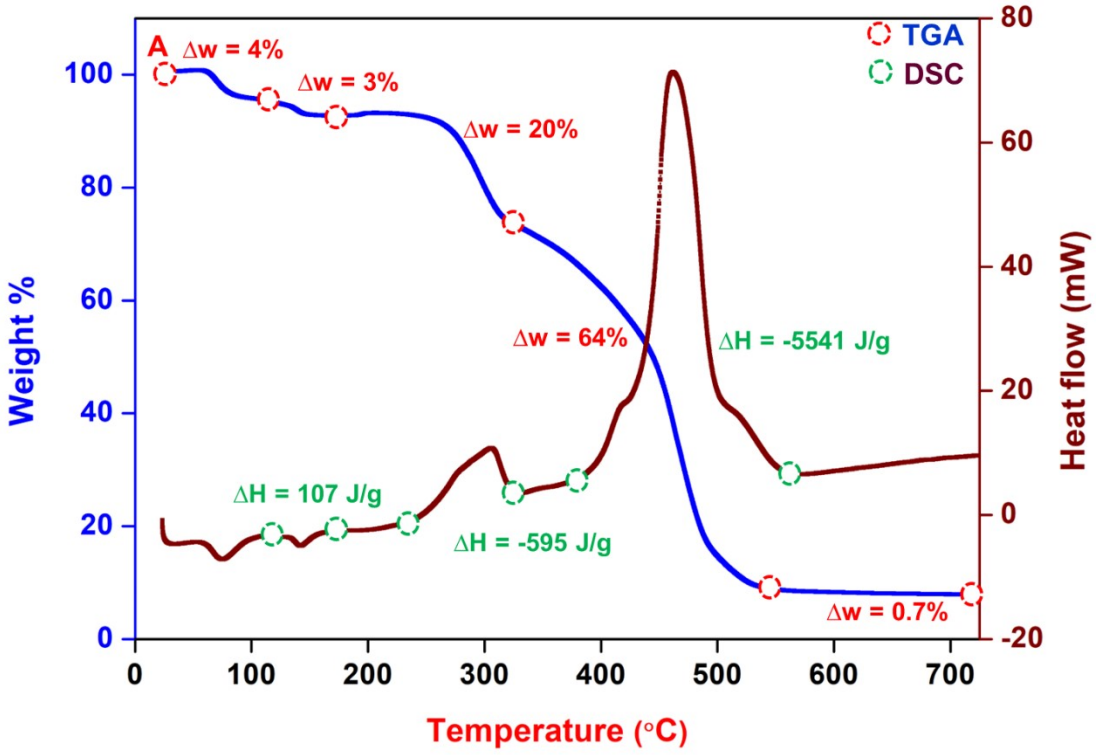
A
Δw = 4%
Δw = 3%
Δw = 20%
Δw = 64%
Δw = 0.7%
ΔH = 107 J/g
ΔH = -595 J/g
ΔH = -5541 J/g
TGA
DSC
Weight %
Heat flow (mW)
Temperature (°C)
0
20
40
60
80
100
-20
0
20
40
60
80
0
100
200
300
400
500
600
700

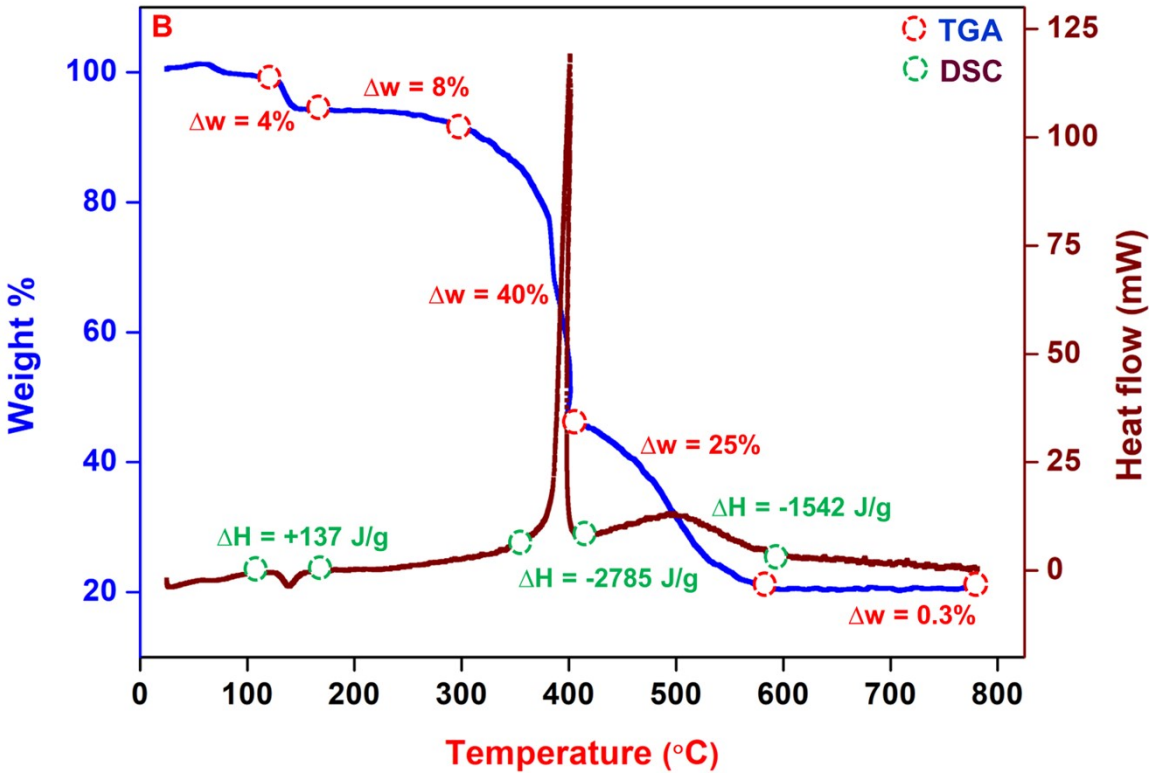

Fig. S9 TG-DSC profiles of (A) **3** and (B) **4**.

Figure S10

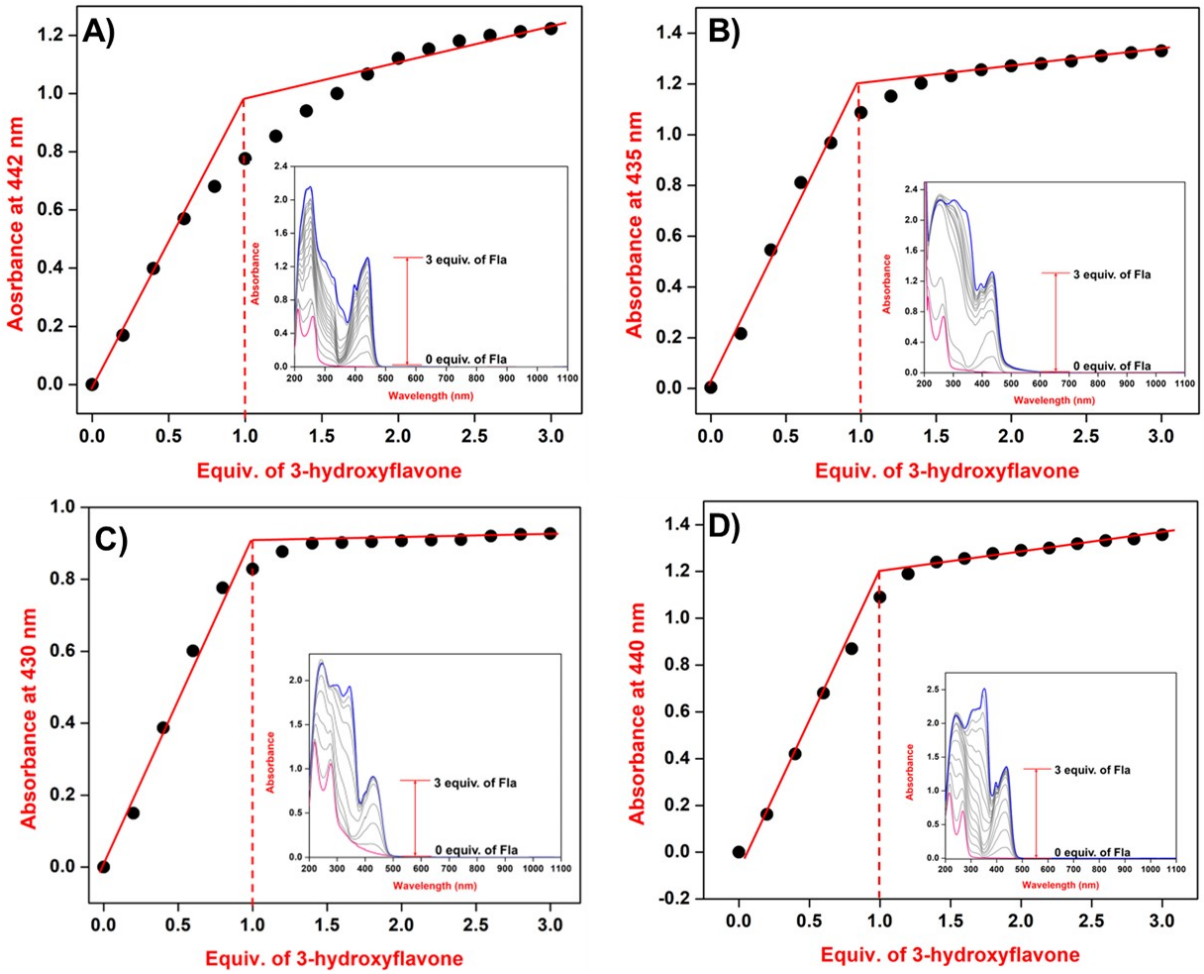

Fig. S10 Spectrophotometric titration curves for the formation of Ni(II)-flavonolate adducts [Ni(II)(L^{H}-L^{Br}(fla)](ClO$_4$) **1–4** upon addition of methanolic solution of flavonolate to the *in situ* generated (A) **1**, (B) **2**, (C) **3** and (D) **4** at 25 °C under N_2 atmosphere. Inset shows the growth of π→π* transition band (~420–430 nm) due to coordinated flavonolate.

Figure S11

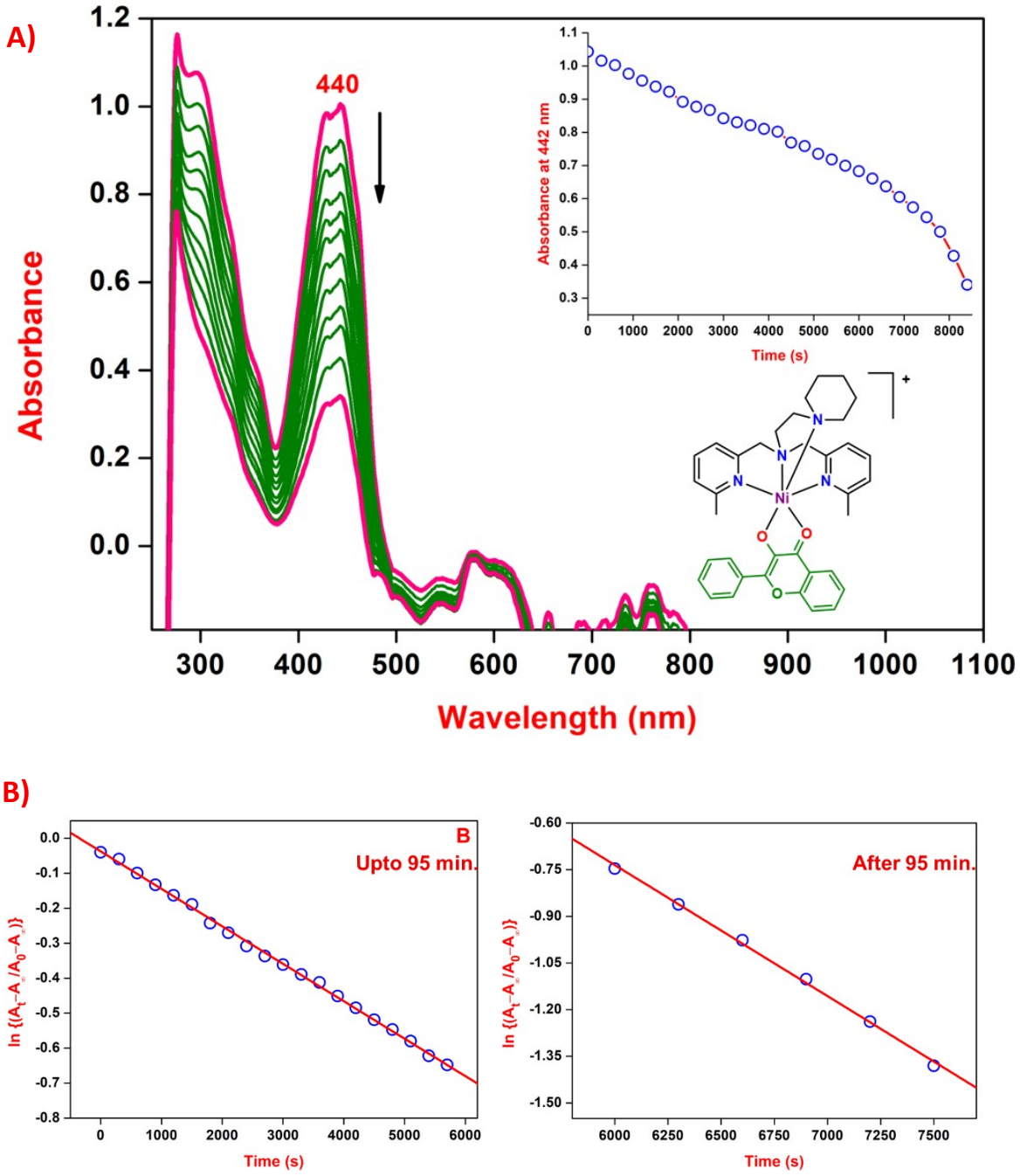

Fig. S11 (A) Electronic absorption spectral changes of **2** monitored at 442 nm in DMF under O_2 atmosphere at 70 °C. Inset shows the time trace of the reaction. (B) Plot of time vs ln{$(A_t–A_0)/(A_t–A_\infty)$}.

Figure S12

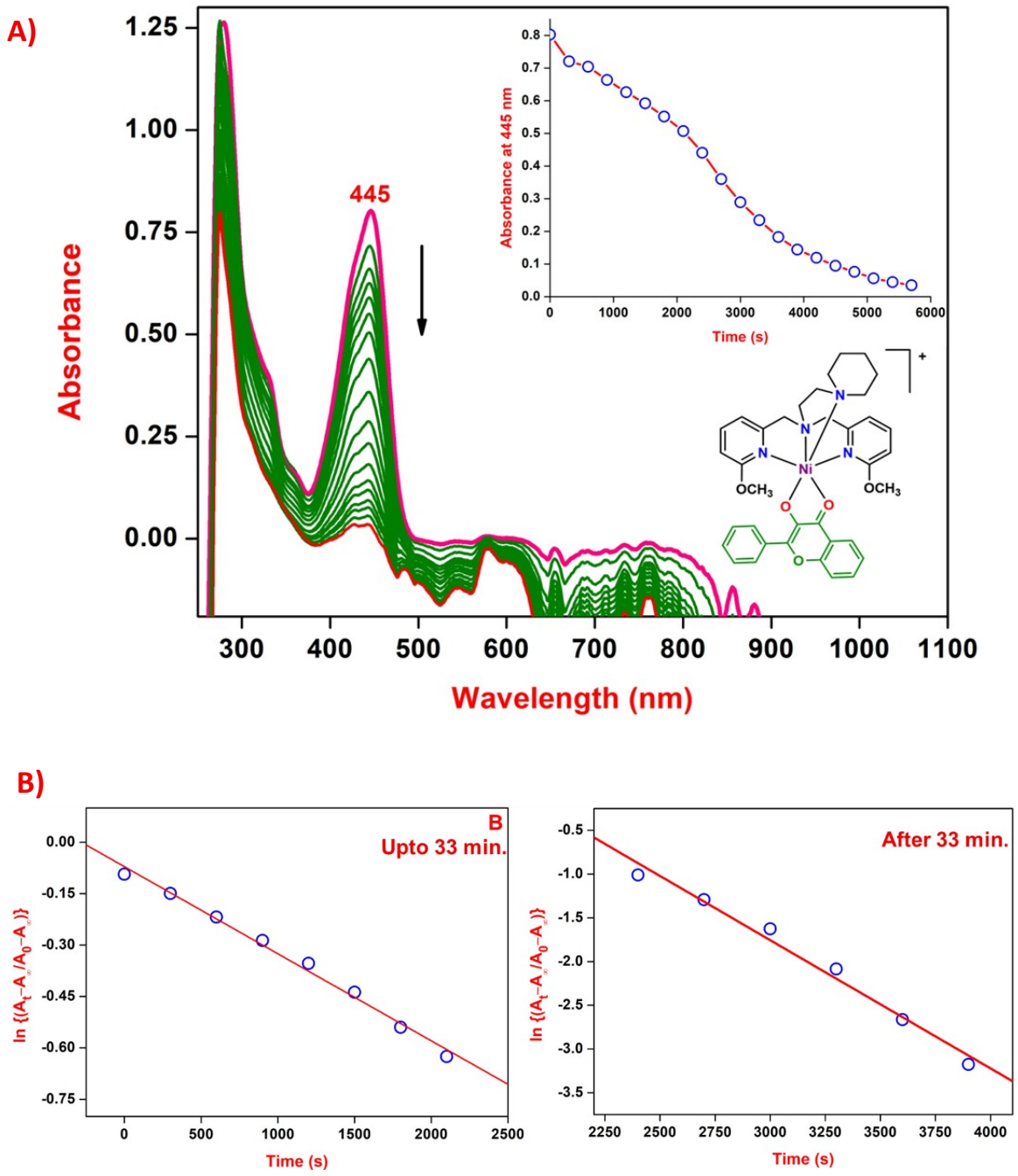

Fig. S12 (A) Electronic absorption spectral changes of **3** monitored at 442 nm in DMF under O_2 atmosphere at 70 °C. Inset shows the time trace of the reaction. (B) Plot of time vs ln{$(A_t–A_0)/(A_t–A_\infty)$}.

Figure S13

A)

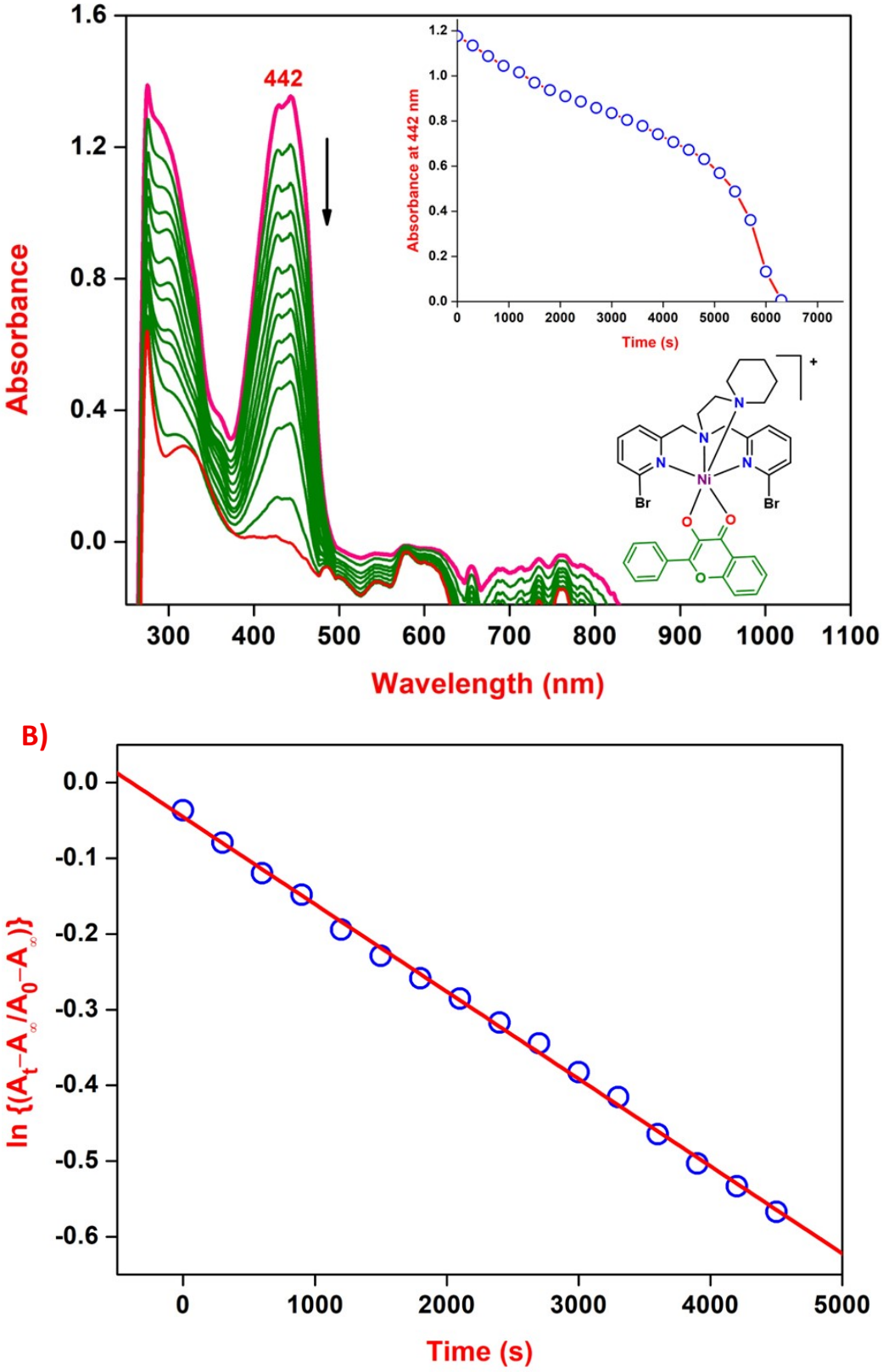

Fig. S13 (A) Electronic absorption spectral changes of **4** monitored at 442 nm in DMF under O_2 atmosphere at 70 °C. Inset shows the time trace of the reaction. (B) Plot of time vs ln{(A_t–A_0)/(A_t–A_∞).

Figure S14

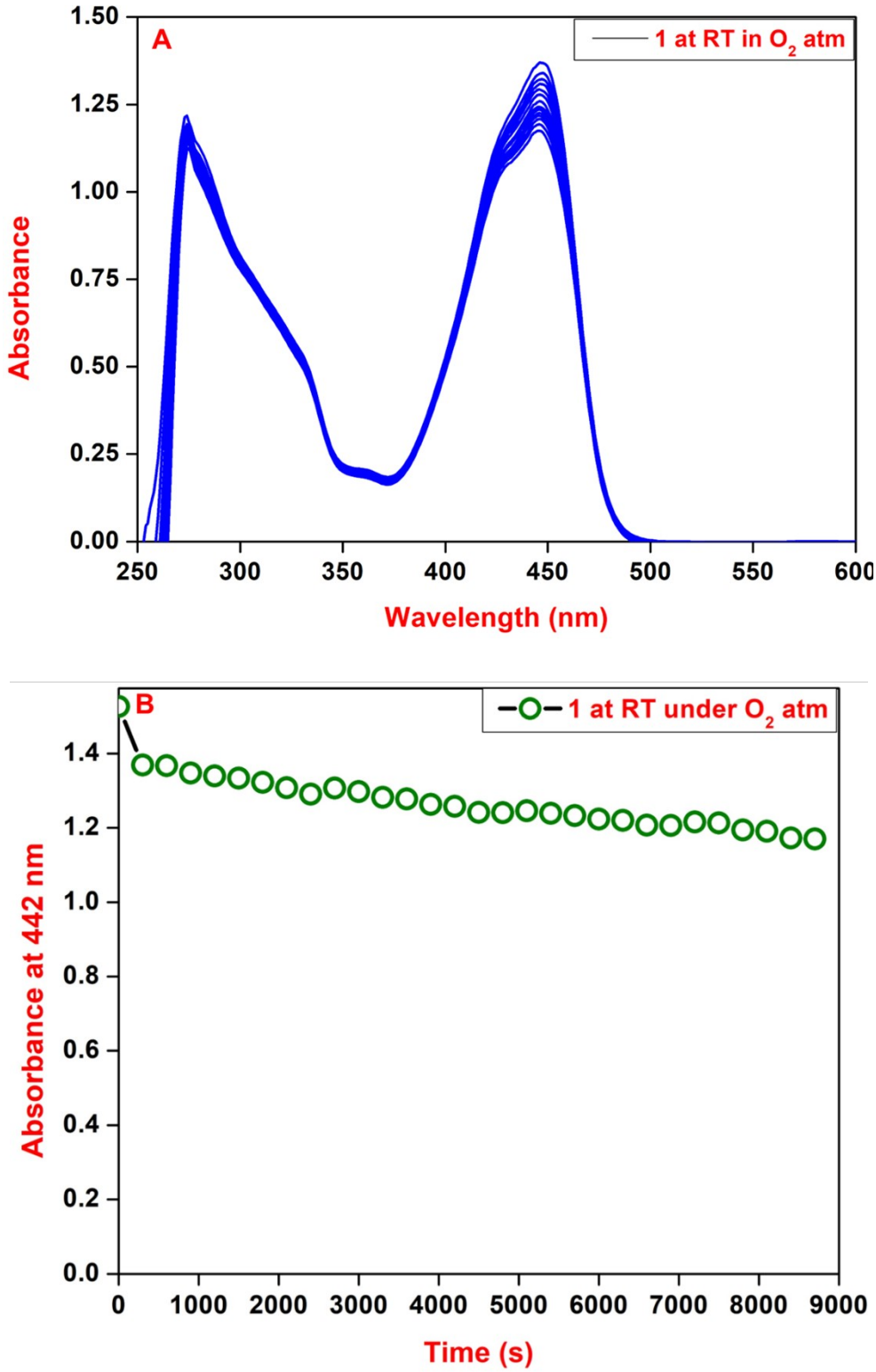

Fig. S14. (A) Electronic absorption spectral changes of **1** tracked at 442 nm in DMF at 25 °C in the presence of O_2. (B) Time trace of the reaction.

Figure S15

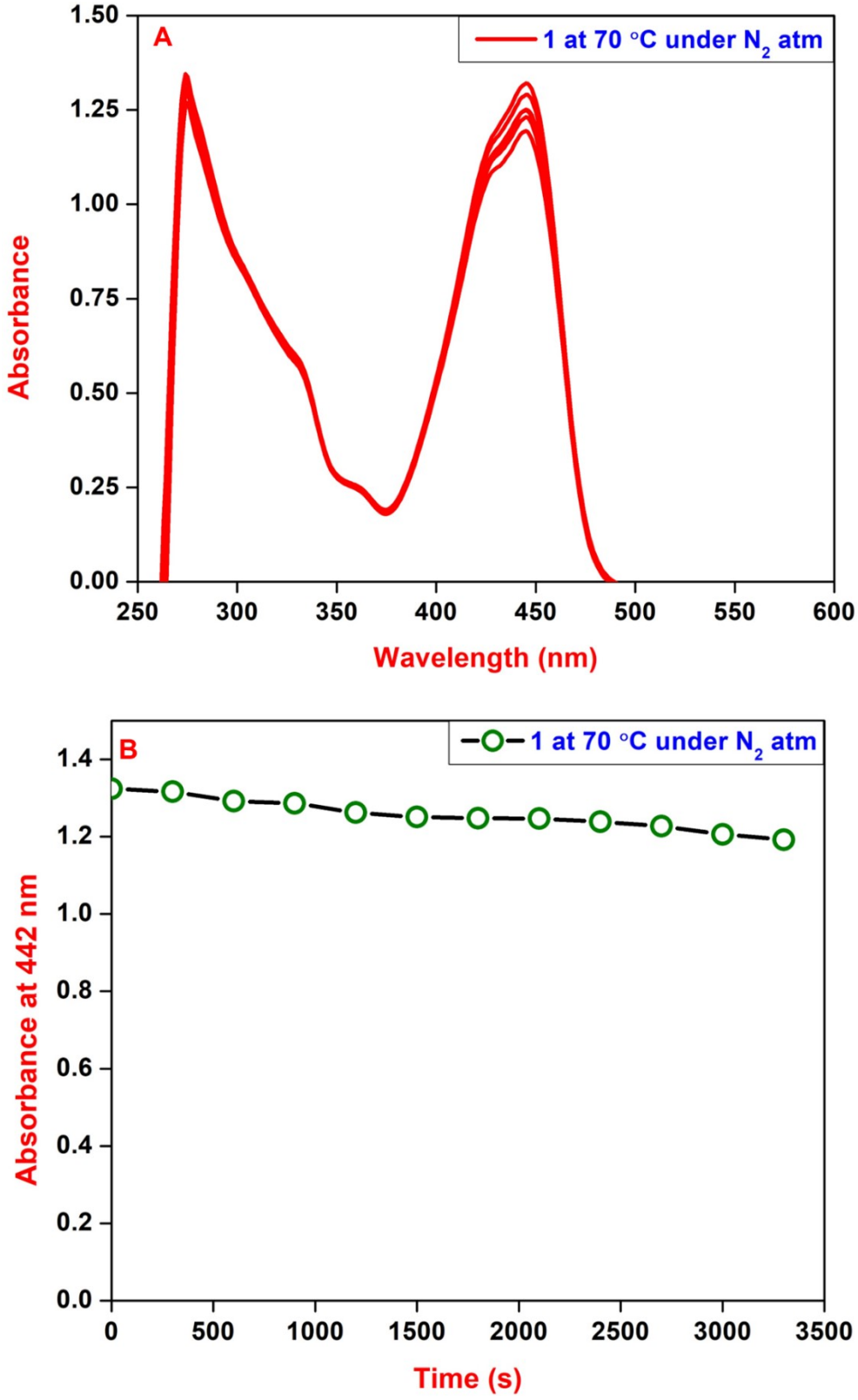

Fig. S15 (A) Electronic absorption spectral changes of [Ni($\mathbf{L^H}$)fla](ClO_4) **1** followed at 442 nm in DMF under N_2 atmosphere at 70 °C. (B) Time trace of the reaction.

Figure S16

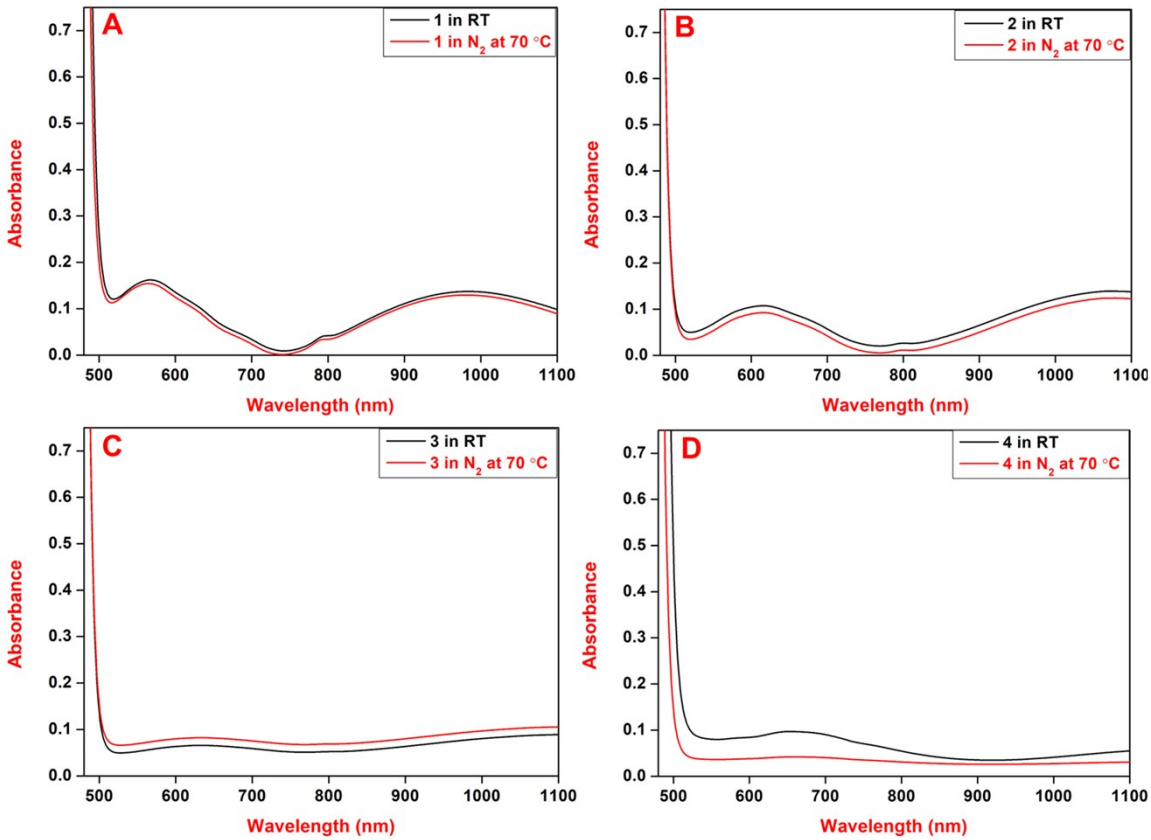

Fig. S16 (A) Electronic absorption spectral measurements of [Ni(**L^{H}–L^{Br}**)fla]$^{+}$ **1–4** tracked at 25 °C (**black**) and 70 °C under N_2 atm (**red**).

Figure S17

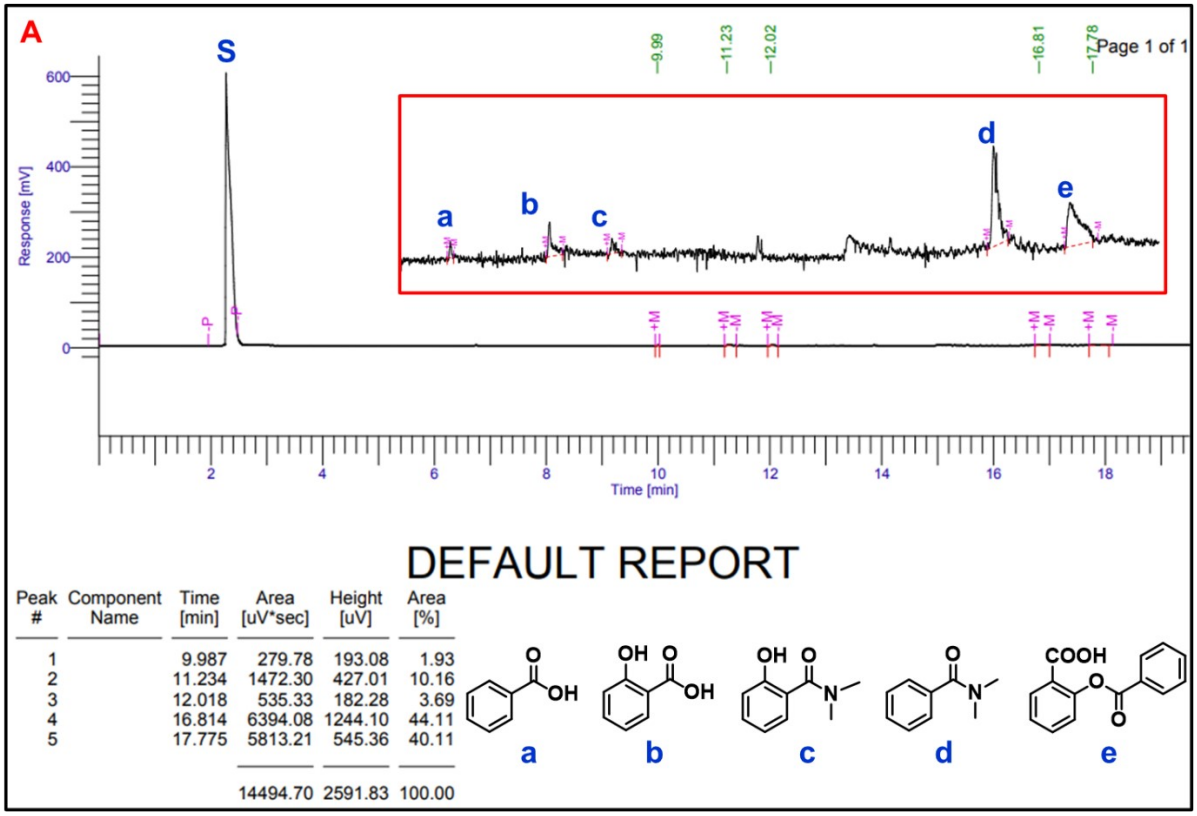

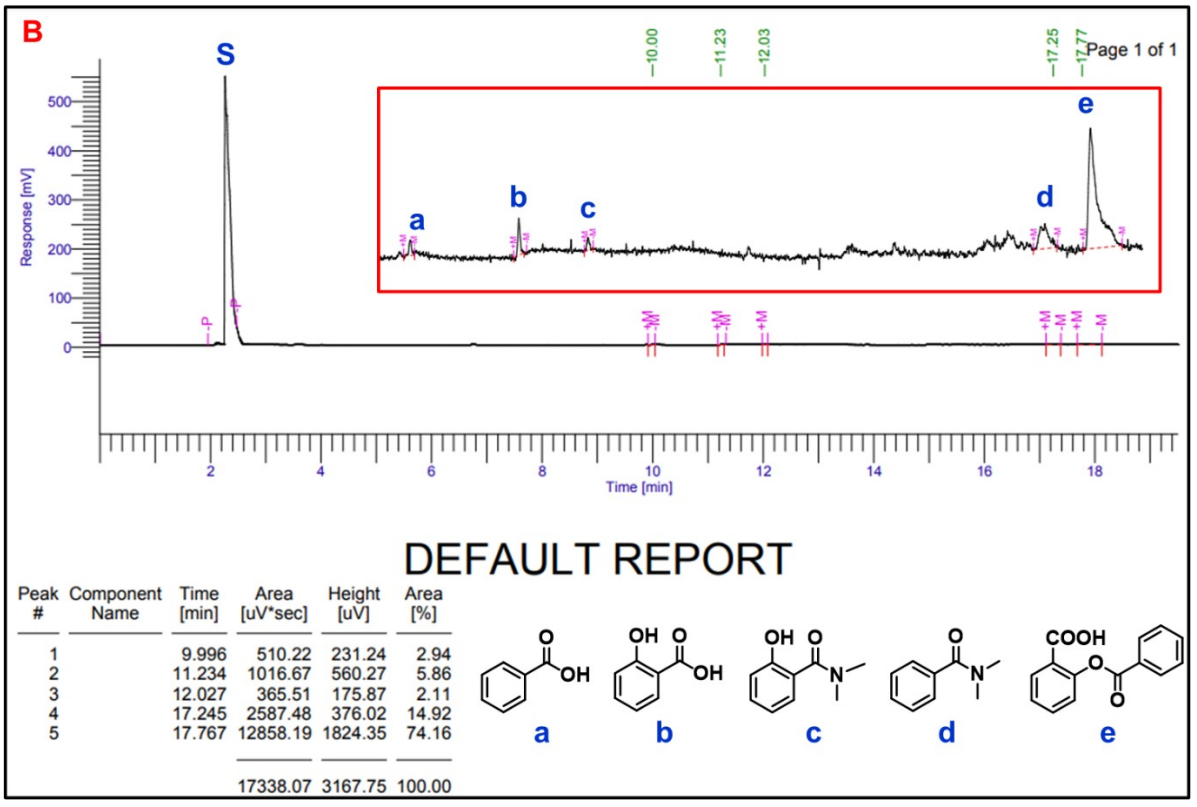

Fig. S17 Gas chromatogram of the product solution of [Ni($\mathbf{L^H}$)(fla)]ClO_4 **1** (A) and [Ni($\mathbf{L^{Me}}$)(fla)]ClO_4 **2** (B) in CH_3OH.

Figure S18

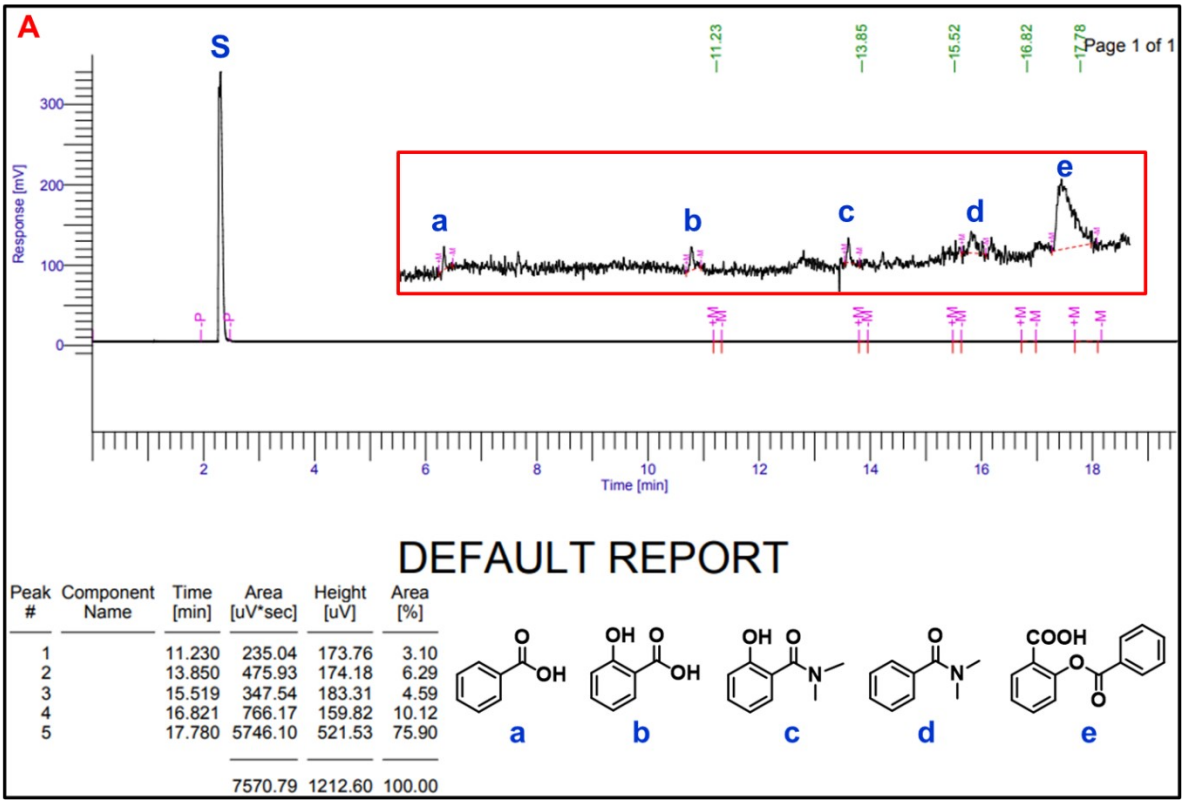

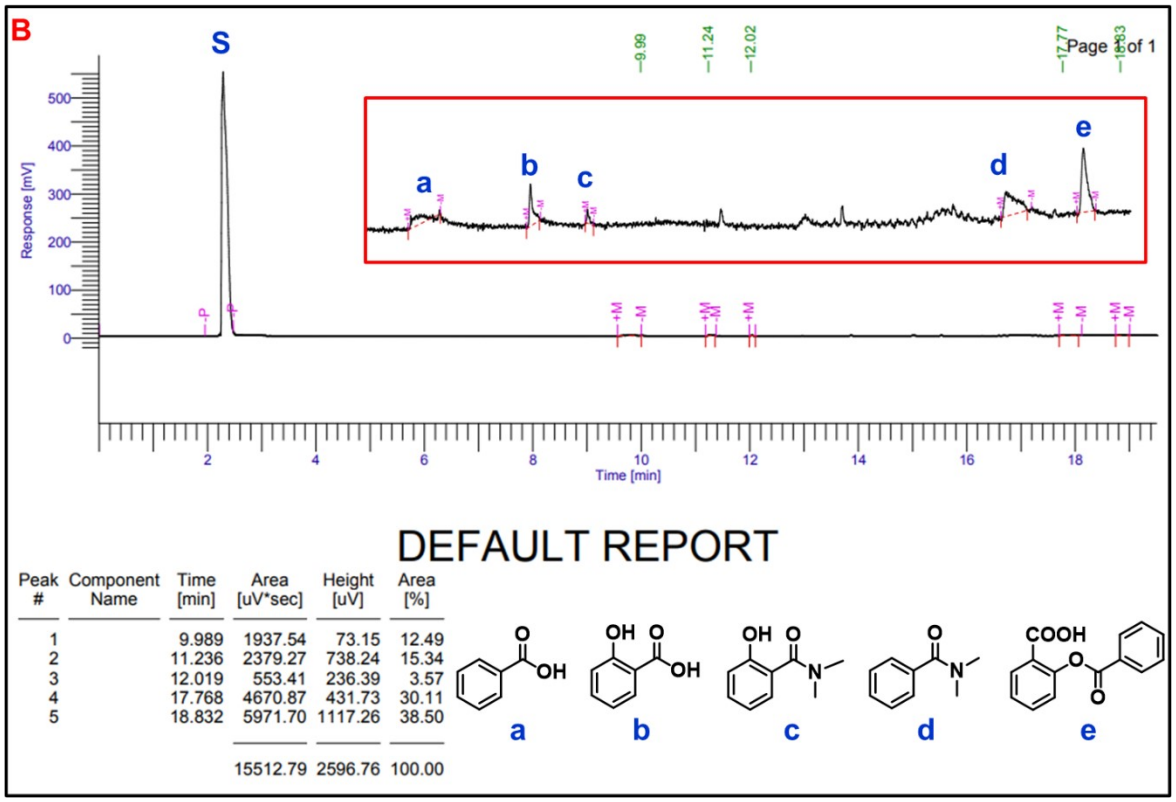

Fig. S18 Gas chromatogram of the product solution of [Ni($\mathbf{L^{Me}}$)(fla)]ClO_4 **3** (A) and [Ni($\mathbf{L^{Br}}$)(fla)]ClO_4 **4** (B) in CH_3OH.

Figure S19

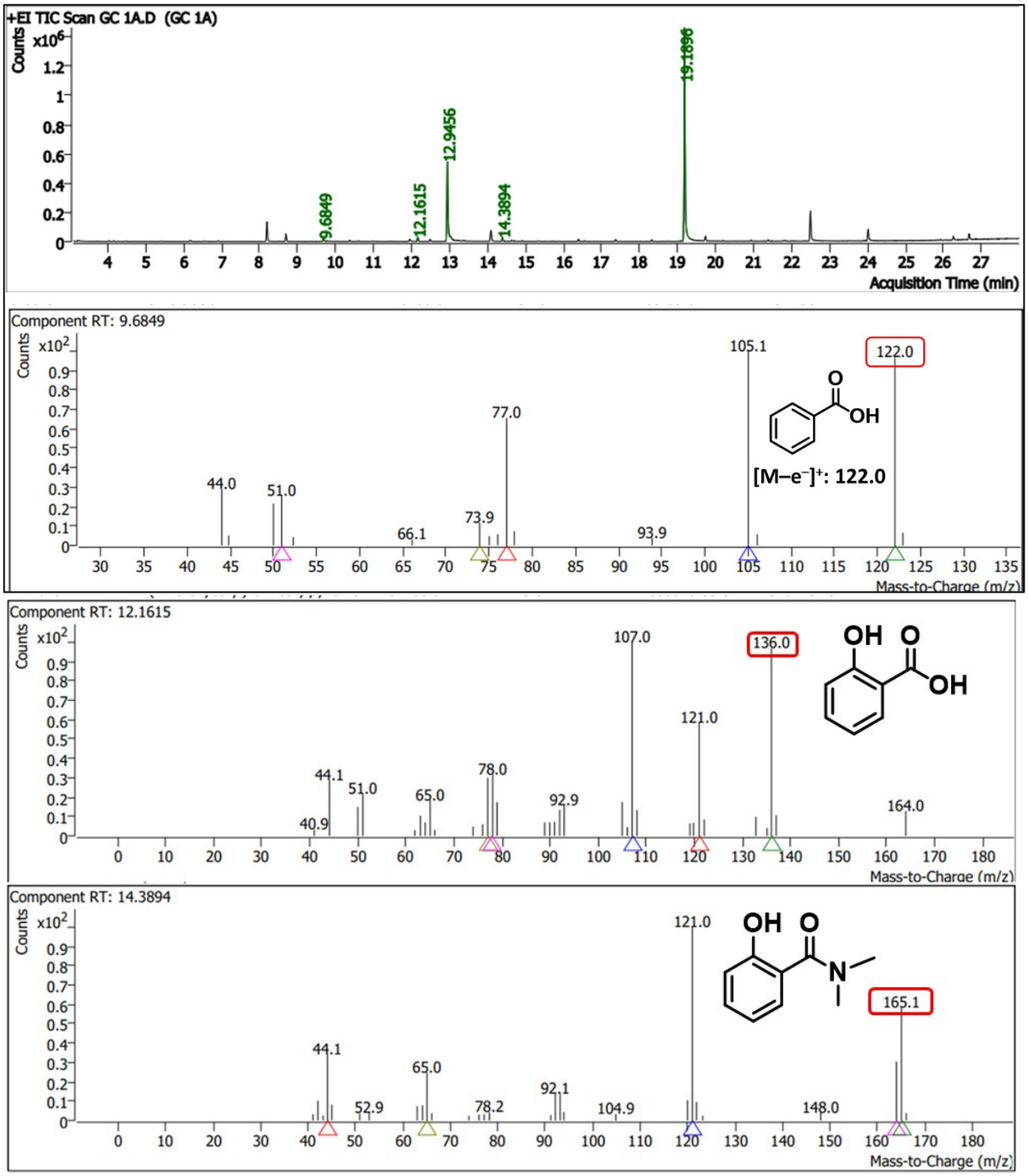

Fig. S19 GC-MS profile of the product solution of [Ni(**L**^{Br})(fla)]ClO_4 **4** in CH_3OH.

Figure S19a

Fig. S19a GC-MS profile of the product solution of [Ni(**L**^{Br})(fla)]ClO_4 **4** in CH_3OH.

Figure S20

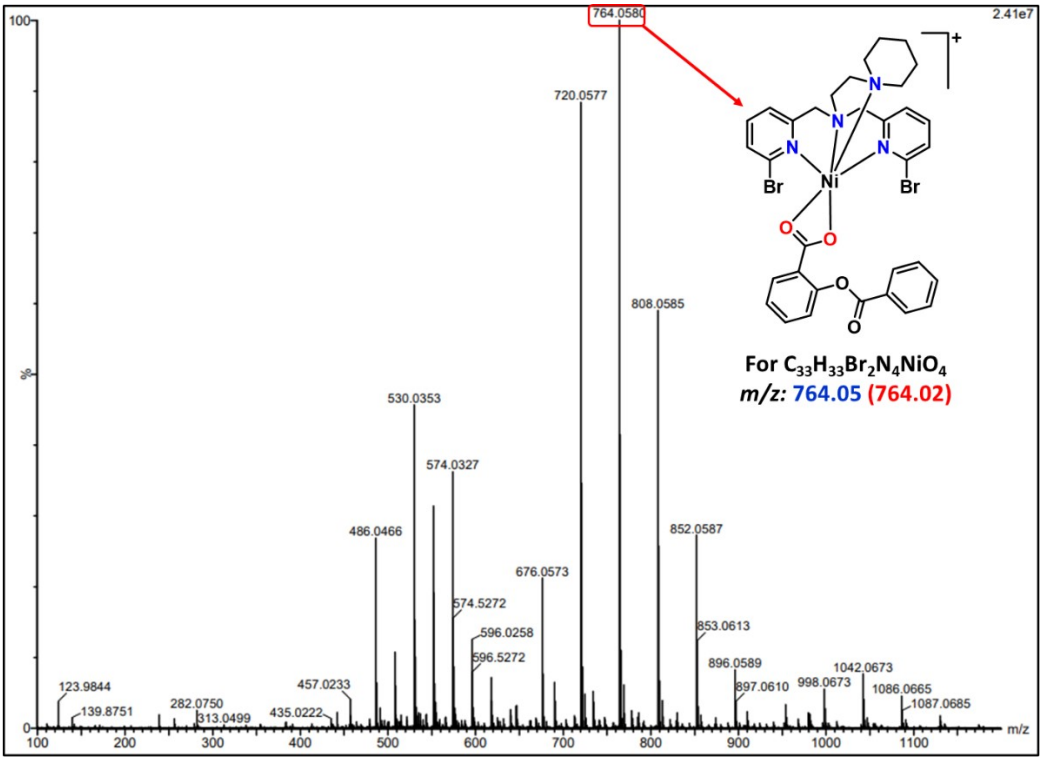

Fig. S20 ESI-MS profile of kinetic product solution of [Ni($\mathbf{L^{Br}}$)(fla)]ClO_4 **4** recorded in CH_3OH.

Figure S21

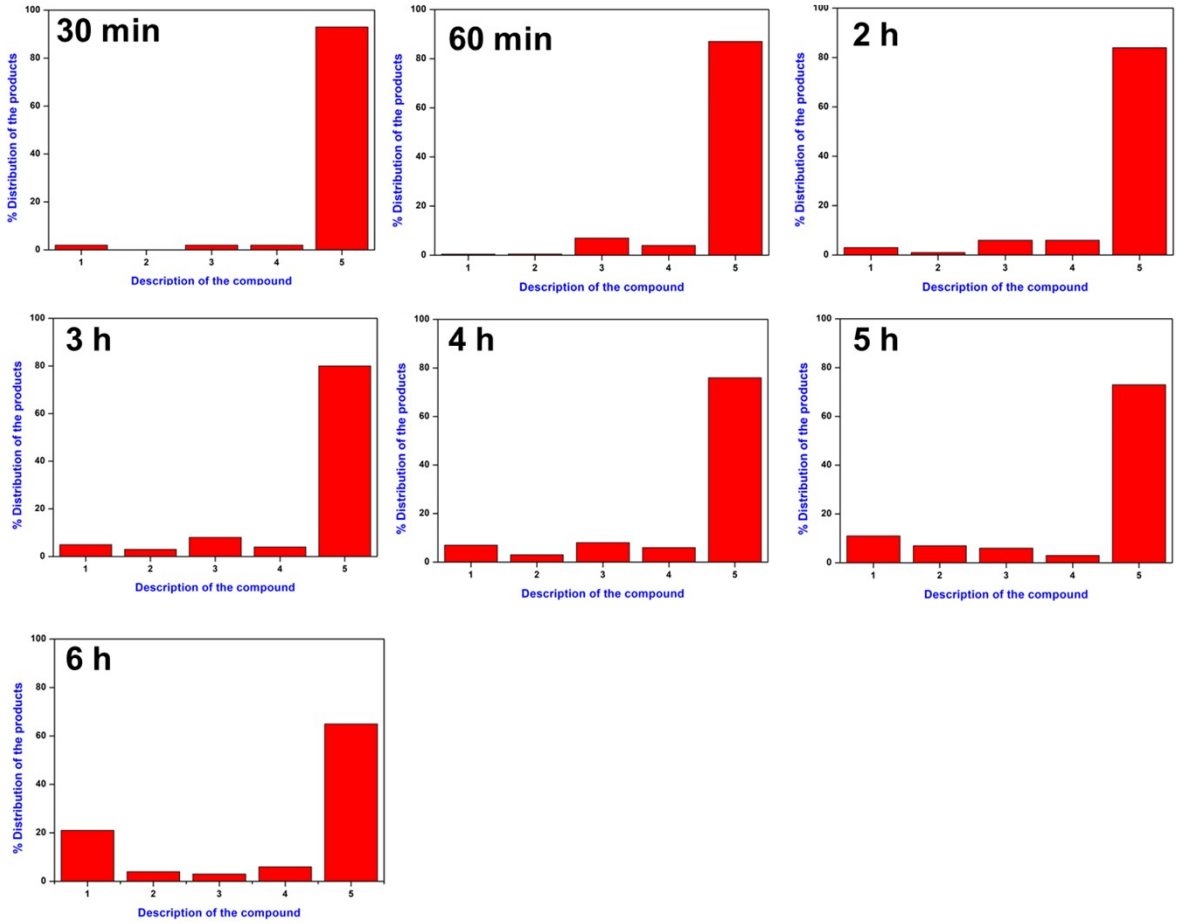

Fig. S21 Time-dependent product analysis of [Ni($\mathbf{L}^{\mathbf{OMe}}$)(fla)]$ClO_4$ **3** recorded in CH_3OH at various time intervals (30 min to 6 h).

Figure S22

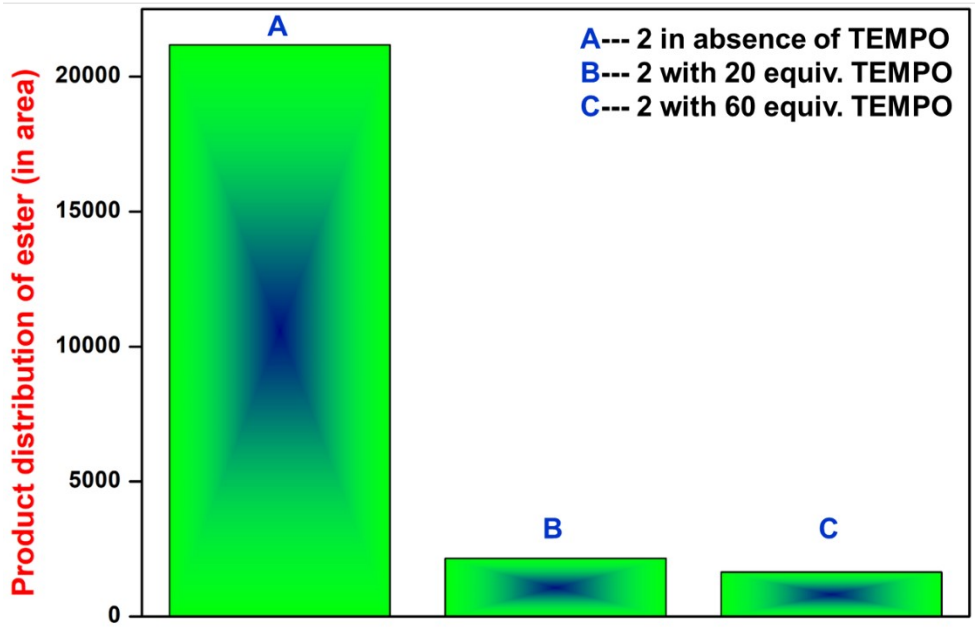

Fig. S22 Time-dependent product analysis of [Ni(**L**^{OMe})(fla)]ClO_4 **3** in the absence and presence of different equiv. of TEMPO recorded in CH_3OH.

Table S1

Table S1. ATR-FTIR spectral data of ligands (L^{H}–L^{Br}) and their corresponding nickel(II)-flavonolate adducts **1–4**.

Functional group	IR Stretching frequency (cm^{-1})							
	L^{H}	**1**	L^{Me}	**2**	L^{OMe}	**3**	L^{Br}	**4**
ν(C=O)	-	1550	-	1550	-	1548	-	1544
ν(C–H)	2938	3093	2929	3087	2939	2981	2968	3070
ν(C=N)	1588	1572	1597	1587	1580	1570	1590	1570
ν(C–N)	1370	1228	1353	1230	1305	1220	1361	1214
ν(O–H)	3375	3578	3364	3544	3380	3468	3396	3466